Chemical Engineering Science 90 (2013) 17–31

Contents lists available at SciVerse ScienceDirect

Chemical Engineering Science

journal homepage: www.elsevier.com/locate/ces

Analysis and numerical investigation of two dynamic models for liquid chromatography

Shumaila Javeed [a,b,c], Shamsul Qamar [a,b,*], Waqas Ashraf [b], Gerald Warnecke [c], Andreas Seidel-Morgenstern [a]

[a] Max Planck Institute for Dynamics of Complex Technical Systems, Sandtorstrasse 1, 39106 Magdeburg, Germany
[b] Department of Mathematics, COMSATS Institute of Information Technology, Park Road Chak Shahzad Islamabad, Pakistan
[c] Institute for Analysis and Numeric, Otto-von-Guericke University, 39106 Magdeburg, Germany

HIGHLIGHTS

- The equilibrium dispersive and lumped kinetic chromatographic models are studied.
- The first three moments for both models are analytically and numerically calculated.
- A close connection between the models is analyzed for linear adsorption isotherms.
- The discontinuous Galerkin (DG) method is applied to solve lumped kinetic model.
- Results of DG-method are compared with analytical and finite volume schemes results.

ARTICLE INFO

Article history:
Received 27 August 2012
Received in revised form
23 November 2012
Accepted 6 December 2012
Available online 19 December 2012

Keywords:
Chromatographic models
Moments analysis
Discontinuous Galerkin method
Dynamic simulation
Adsorption
Mass transfer

ABSTRACT

This paper presents the analytical and numerical investigations of two established models for simulating liquid chromatographic processes namely the equilibrium dispersive and lumped kinetic models. The models are analyzed using Dirichlet and Robin boundary conditions. The Laplace transformation is applied to solve these models analytically for single component adsorption under linear conditions. Statistical moments of step responses are calculated and compared with the numerical predictions for both types of boundary conditions. The discontinuous Galerkin finite element method is proposed to numerically approximate the more general lumped kinetic model. The scheme achieves high order accuracy on coarse grids, resolves sharp discontinuities, and avoids numerical diffusion and dispersion. For validation, the results of the suggested method are compared with some flux-limiting finite volume schemes available in the literature. A good agreement of the numerical and analytical solutions for simplified cases verifies the robustness and accuracy of the proposed method. The method is also capable to solve chromatographic models also for non-linear and competitive adsorption equilibrium isotherms.

1. Introduction

Chromatography is a highly selective separation and purification process used in a broad range of industries, including pharmaceutical and biotechnical applications. In recent years, this technology emerged as a useful tool to isolate and purify chiral molecules, amino-acids, enzymes, and sugars. It has capability to provide high purity and yield at reasonable production rates even for difficult separations, for instance to isolate enantiomers or to purify proteins. During the migration of the mixture components through tubular columns filled with suitable particles forming the stationary phase, composition fronts develop and propagate governed by the adsorption isotherms providing a characteristic retention behavior of the species involved. Separated peaks of desired purity can be collected periodically at the outlet of the columns.

Different models were introduced in the literature for describing chromatographic processes, such as the general rate model, various kinetic models, and the equilibrium dispersive model (EDM), see e.g. Ruthven (1984), Guiochon and Lin (2003), Felinger et al. (2004), and Guiochon et al. (2006).

In this paper, the EDM and a non-equilibrium adsorption lumped kinetic model (LKM), suggested initially by Lapidus and Amundson (1952), are solved analytically and numerically. For this purpose, the Laplace transformation is utilized as a basic tool to transform the partial differential equations (PDEs) of the models for linear isotherms to ordinary differential equations (ODEs). The corresponding analytical solutions of EDM and LKM are obtained along with Dirichlet and Robin boundary conditions. If no analytical

* Corresponding author at: Max Planck Institute for Dynamics of Complex Technical Systems, Sandtorstrasse 1, 39106 Magdeburg, Germany.
Tel.: +49 391 6110454; fax: +49 391 6110500.
E-mail addresses: javeed@mpi-magdeburg.mpg.de (S. Javeed), qamar@mpi-magdeburg.mpg.de, shamsul.qamar@comsats.edu.pk (S. Qamar).

0009-2509/$ - see front matter © 2012 Elsevier Ltd. All rights reserved.
http://dx.doi.org/10.1016/j.ces.2012.12.014

inversion could be performed, the numerical inversion is used to generate the time domain solution for both types of boundary conditions. To analyze the considered models, the moment method is employed to get expressions for retention times, band broadenings, and front asymmetries. Such moment analysis approach has been found instructive in the literature, see for example Guiochon et al. (2006), Kubib (1965a,b), Kucera (1965), Miyabe and Guiochon (2000, 2003), Miyabe (2007, 2009), Ruthven (1984), Schneider and Smith (1968) as well as Suzuki (1973).

For non-linear adsorption isotherms, analytical solutions of the model equations cannot be derived. For that reason, numerical simulations are needed to accurately predict the dynamic behavior of chromatographic columns. Steep concentration fronts and shock layers may occur due to the convection dominated PDEs of chromatographic models and, hence, an efficient numerical method is required to obtain accurate and physically realistic solutions.

Discontinuous Galerkin (DG) methods have been widely used in the computational fluid dynamics and could be a good choice to solve non-linear convection-dominated problems, see e.g. Bassi and Rebay (1997), Bahhar et al. (1998), Aizinger et al. (2000), Holik (2009). This method was introduced by Reed and Hill (1973) for hyperbolic equations. Afterwards, various DG methods were developed and formulated for non-linear hyperbolic systems, see for example Cockburn and Shu (1989, 1998, 2001), Cockburn et al. (1990). The DG methods are robust, high order accurate and stable. They use discontinuous approximations which incorporate the ideas of numerical fluxes and slope limiters in a very natural way to avoid oscillations in the region of sharp variations. Their highly parallelizable nature make them easily applicable to complicated geometries and boundary conditions. In this work, the Runge–Kutta discontinuous Galerkin (RKDG) method is for the first time applied to solve the more general lumped kinetic chromatographic model. The scheme uses the DG scheme in space coordinates that converts the given PDEs of the model to a system of ODEs. An explicit and non-linearly stable high order Runge–Kutta method is used to solve the resulting ODEs system. The scheme satisfies the total variation bounded (TVB) property that guarantees the positivity of the scheme, for example the non-negativity of the mixture concentrations in the current study.

This paper is arranged as follows. In Section 2, the non-equilibrium lumped kinetic model and as its special case the equilibrium dispersive model are introduced. In Section 3, analytical solutions of the two models are discussed. In Section 4, the RKDG method is derived. In Section 5, the results of the moment analysis are presented for the considered models. Numerical test problems are discussed in Section 6 including the case of binary mixtures for non-linear conditions. Finally, Section 7 gives the conclusions.

2. The lumped kinetic model (LKM)

The following assumptions are used in the derivation of LKM:

1. The column is packed homogeneously and is isothermal.
2. The radial gradients of concentrations in the column are neglected.
3. The volumetric flow rate remains constant.
4. The model lumps contribution of internal and external mass transport resistances with a mass transfer coefficient k.
5. Additionally, the axial dispersion coefficient D is considered constant for all components.

In the light of above assumptions, the mass balance laws of a multi-component LKM are expressed as

$$\frac{\partial c_n}{\partial t}+u\frac{\partial c_n}{\partial z}=D\frac{\partial^2 c_n}{\partial z^2}-\frac{k}{\epsilon}(q_n^*-q_n), \tag{1}$$

$$\frac{\partial q_n}{\partial t}=\frac{k}{1-\epsilon}(q_n^*-q_n), \tag{2}$$

$$q_n^*=f(c_n), \quad n=1,2,\ldots,N_c. \tag{3}$$

In the above equations, N_c represents the number of mixture components in the sample, c_n denotes the n-th liquid concentration, q_n is the n-th solid concentration, u is the interstitial velocity, ϵ is porosity, t is time, and z stands for the axial-coordinate. The three characteristic times in the model Eq. (1) are defined as

$$\tau_C=\frac{L}{u}, \quad \tau_D=\frac{D}{u^2}, \quad \tau_{MT}=\frac{1}{k}. \tag{4}$$

The ratios of these characteristic times provide dimensionless quantities as

$$\tilde{\tau_1}=\frac{\tau_C}{\tau_D}=\frac{Lu}{D}, \quad \tilde{\tau_2}=\frac{\tau_C}{\tau_{MT}}=\frac{Lk}{u}. \tag{5a}$$

Here, $\tilde{\tau_1}$ typically is frequently called the Peclet number Pe

$$Pe=\tilde{\tau_1}=\frac{Lu}{D}, \tag{5b}$$

where L denotes the length of the column.

In Eq. (3), the isotherm q_n^* describes an equilibrium relationship between the concentrations of n-th components in the stationary and mobile phases. Isotherms provide thermodynamic information for designing a chromatographic separation process, while a non-linear isotherm describes a non-linear relationship between the liquid and solid phases. The frequently applied convex non-linear Langmuir isotherm is defined as

$$q_n^*=\frac{a_n c_n}{1+\sum_{\tilde{n}=1}^{N_c} b_{\tilde{n}} c_{\tilde{n}}}, \quad n=1,2,\ldots,N_c, \tag{6}$$

where the a_n represent Henry's coefficients and the $b_{\tilde{n}}$ quantify the non-linearity of the single component isotherms. For diluted systems or small concentrations, Eq. (6) reduces to linear isotherms

$$q_n^*=a_n c_n, \quad n=1,2,3,\ldots,N_c. \tag{7}$$

In above equations, a_n denotes the n-th Henry's coefficient. The initial conditions for fully regenerated columns are given as

$$c_n(0,z)=0, \quad q_n(0,z)=0. \tag{8}$$

To solve Eqs. (1)–(3), inflow and outflow boundary conditions (BCs) are required. Two types of boundary conditions are applied in this paper to solve the above model.

2.1. Boundary conditions of type I: Dirichlet boundary conditions

For sufficiently small dispersion coefficient, for example $D=10^{-5}$ m^2/s, the Dirichlet boundary conditions can be used at the column inlet

$$c_n|_{z=0}=c_{n,0}. \tag{9a}$$

A useful and realistic outlet boundary conditions are

$$c_n(\infty,t)=0. \tag{9b}$$

2.2. Boundary conditions of type II: Robin type boundary conditions

The following accurate inlet boundary conditions are typically used, see e.g. Danckwerts (1953) and Seidel-Morgenstern (1991). This Robin type of boundary conditions is known in chemical engineering as Danckwerts conditions

$$c_n|_{z=0}=c_{n,0}+\frac{D}{u}\frac{\partial c_n}{\partial z}, \quad n=1,2,3,\ldots,N_c. \tag{10a}$$

These inlet conditions are usually applied together with the following outlet conditions:

$$\frac{\partial c_n(L,t)}{\partial z}=0. \tag{10b}$$

Apart from the two sets used in this work, other boundary conditions can also be applied to solve the model Eqs. (1)–(3).

2.3. The equilibrium dispersive model (EDM)—a limiting case of LKM

The basic assumption of EDM is that the kinetics of mass transfer in the chromatographic column and the kinetics of adsorption–desorption are fast. This means, the equilibrium between stationary and mobile phases at all positions of the column is achieved instantaneously. Further, the value of the mass transport coefficient k used in the LKM, Eqs. (1) and (2), becomes larger, i.e. $k\to\infty$, the model Eqs. (1)–(3) change to the equilibrium dispersive model ($\partial q/\partial t=\partial q^*/\partial t$) as given below

$$\frac{\partial c_n}{\partial t}+F\frac{\partial q_n^*}{\partial t}+u\frac{\partial c_n}{\partial z}=D_{\text{app}}\frac{\partial^2 c_n}{\partial z^2},\quad n=1,2,3,\ldots,N_c. \tag{11}$$

Here, F is the phase ratio related to porosity, i.e. $F=(1-\epsilon)/\epsilon$, D_{app} is the apparent dispersion coefficient related to the Peclet number by $Pe=Lu/D_{\text{app}}$.

3. Analytical solutions of EDM and LKM for linear isotherms

In this section, single component ($N_c=1$) linear chromatographic models are considered. Analytical solutions are derived in a Laplace domain for linear isotherms (Eq. (7)) with Dirichlet (Eq. (9a)) and Danckwerts (Eq. (10a)) inlet boundary conditions. To simplify the notations, we consider $c(x,t)=c_1(x,t)$.

3.1. Analytical solution of EDM

The Laplace transformation is defined as

$$C(x,s)=\int_0^\infty \mathrm{e}^{-st}c(x,t)\,dt,\quad s>0. \tag{12}$$

After normalizing Eq. (11) by defining

$$x=z/L,\quad Pe=Lu/D_{\text{app}} \tag{13}$$

and by applying the Laplace transformation (12) to Eq. (11) with $N_c=1$ and $c_{\text{init}}(t=0,z)=0$, we obtain

$$\frac{\partial^2 C}{\partial x^2}-Pe\,\frac{\partial C}{\partial x}-s\,Pe\,\frac{L}{u}(1+aF)C=0. \tag{14}$$

The solution of this equation is given as

$$C(x,s)=A\exp(\lambda_1 x)+B\exp(\lambda_2 x), \tag{15}$$

$$\lambda_{1,2}=\frac{Pe}{2}\mp\frac{1}{2}\sqrt{Pe^2+4\,Pe\,\frac{L}{u}(1+aF)s}. \tag{16}$$

After applying the Dirichlet boundary conditions in Eqs. (9a) and (9b), the values of A and B are given as

$$A=\frac{c_0}{s},\quad B=0. \tag{17}$$

Then, Eq. (15) takes the following simple form:

$$C(x,s)=\frac{c_0}{s}\exp\left(\frac{Pe}{2}-\frac{1}{2}\sqrt{Pe^2+4\,Pe\,\frac{L}{u}(1+aF)s}\right)x. \tag{18}$$

The solution in the time domain $c(x,t)$, can be obtained by using the exact formula for the back transformation as

$$c(x,t)=\frac{1}{2\pi i}\int_{\gamma-i\infty}^{\gamma+i\infty}\mathrm{e}^{ts}C(x,s)\,ds, \tag{19}$$

where γ is a real constant that exceeds the real part of all the singularities of $C(x,s)$. On applying Eq. (19) to Eq. (18), we obtain

$$c(x,t)=\frac{c_0}{2}\,\mathrm{erfc}\left(\frac{\sqrt{\frac{Pe}{2}}L/u(1+aF)x-t}{\sqrt{\frac{L}{u}t(1+aF)}}\right)+\frac{c_0}{2}\exp(x\,Pe)\,\mathrm{erfc}\left(\frac{\sqrt{\frac{Pe}{2}}L/u(1+aF)x+t}{\sqrt{\frac{L}{u}t(1+aF)}}\right), \tag{20}$$

where erfc denotes the complementary error function.

If we consider the second set of boundary conditions given by Eqs. (10a) and (10b), the values of A and B take the following forms:

$$A=\frac{c_0}{s}\frac{\lambda_2\exp(\lambda_2)}{\left(1-\frac{\lambda_1}{Pe}\right)\lambda_2\exp(\lambda_2)-\left(1-\frac{\lambda_2}{Pe}\right)\lambda_1\exp(\lambda_1)}, \tag{21}$$

$$B=\frac{-c_0}{s}\frac{\lambda_1\exp(\lambda_1)}{\left(1-\frac{\lambda_1}{Pe}\right)\lambda_2\exp(\lambda_2)-\left(1-\frac{\lambda_2}{Pe}\right)\lambda_1\exp(\lambda_1)}. \tag{22}$$

With these values A and B, the back transformation of Eq. (15) is not doable analytically. However, well established numerical inverse Laplace transformation could be used to get $c(x,t)$. In this paper, the Fourier series approximation of Eq. (19) is used, see e.g. Rice and Do (1995).

3.2. Analytical solution of LKM

After applying the Laplace transformation to the single component LKM with Dirichlet boundary conditions, Eqs. (1) and (2) take the forms

$$\frac{\partial^2 C}{\partial x^2}-Pe\,\frac{\partial C}{\partial x}-\frac{Pe\,L}{u}Cs-\frac{L^2}{\epsilon D}akC+\frac{L^2}{\epsilon D}kQ=0, \tag{23}$$

$$sQ=\frac{k}{1-\epsilon}(aC-Q)\Rightarrow Q=\frac{\frac{ka}{(1-\epsilon)}}{s+\frac{k}{(1-\epsilon)}}C. \tag{24}$$

On putting the value of Q in Eq. (23), we obtain

$$\frac{\partial^2 C}{\partial x^2}-Pe\,\frac{\partial C}{\partial x}-Pe\,\frac{L}{u}Cs-\frac{L^2}{\epsilon D}akC+\frac{L^2}{\epsilon D}\frac{\frac{k^2a}{(1-\epsilon)}}{s+\frac{k}{(1-\epsilon)}}C=0 \tag{25}$$

or

$$\frac{\partial^2 C}{\partial x^2}-Pe\,\frac{\partial C}{\partial x}-\left(Pe\,\frac{L}{u}s-\frac{L^2}{\epsilon D}\frac{\frac{k^2a}{(1-\epsilon)}}{s+\frac{k}{(1-\epsilon)}}+\frac{L^2}{\epsilon D}ak\right)C=0. \tag{26}$$

Thus, the Laplace domain solution is given as

$$C(x,s)=A\exp(\lambda_1 x)+B\exp(\lambda_2 x), \tag{27}$$

where

$$\lambda_{1,2} = \frac{Pe}{2} \mp \sqrt{\left(\frac{Pe}{2}\right)^2 + \left(Pe\frac{L}{u}s - \frac{L^2}{\epsilon D}\frac{\frac{k^2 a}{(1-\epsilon)}}{s+\frac{k}{(1-\epsilon)}} + \frac{L^2}{\epsilon D}ak \right)}. \quad (28)$$

For the simplified boundary conditions (9a) and (9b), we have again

$$A = \frac{c_o}{s}, \quad B = 0. \quad (29)$$

Using these values of A and B in Eq. (27), we obtain

$$C(x,s) = \frac{c_o}{s}\exp\left(\frac{Pe}{2} - \sqrt{\left(\frac{Pe}{2}\right)^2 + \left(Pe\,\frac{L}{u}s - \frac{L^2}{\epsilon D}\frac{\frac{k^2 a}{(1-\epsilon)}}{s+\frac{k}{(1-\epsilon)}} + \frac{L^2}{\epsilon D}ak \right)}\right)x \quad (30)$$

or

$$C(x,s) = \frac{c_o}{s}\exp\left(\frac{Pe}{2} - \frac{1}{2}\sqrt{Pe^2 + 4\,Pe\,\frac{L}{u}s\left(1+\frac{aF}{1+\frac{s(1-\epsilon)}{k}}\right)}\right)x. \quad (31)$$

For sufficiently large values of k in Eq. (31), i.e. when $k\to\infty$, the transformed solution $C(x,s)$ for LKM becomes the solution of EDM given by Eq. (18). Once again, the numerical inverse Laplace transformation is employed to find the original solution $c(x,t)$ of Eq. (31). For Danckwerts boundary conditions in Eqs. (10a) and (10b), the solution in the Laplace domain takes the same form as given by Eq. (27). The values of A and B are provided by Eqs. (21) and (22), whereas $\lambda_{1,2}$ can be found in Eq. (28). The numerical inverse Laplace transformation was employed to find the original solution $c(x,t)$.

4. Reduced EDM and LKM: moment models

Moment analysis is an effective strategy for deducing important information about the retention equilibrium and mass transfer kinetics in the column, see e.g. Guiochon et al. (2006), Kucera (1965), Miyabe (2007, 2009), Ruthven (1984), Schneider and Smith (1968) as well as Suzuki and Smith (1971). The Laplace transformation can be used as a basic tool to obtain moments. The numerical inverse Laplace transformation of the equations provides the optimum solution, but this solution is not helpful to study the behavior of chromatographic band in the column. The retention equilibrium-constant and parameters of the mass transfer kinetics in the column are related to the moments in the Laplace domain. In this section, a method for describing chromatographic peaks by means of statistical moments is used and the central moments up to third order are calculated for two sets of boundary conditions. The moment of the band profile at the exit of chromatographic bed of length $x=L$ is

$$\mu_i = \int_0^\infty C(x=L,t)t^i\,dt. \quad (32)$$

The i-th initial normalized moment is

$$\mu_i = \frac{\int_0^\infty C(x=L,t)t^i\,dt}{\int_0^\infty C(x=L,t)\,dt}. \quad (33)$$

The i-th central moment is

$$\mu_i' = \frac{\int_0^\infty C(x=L,t)(t-\mu_1)^i\,dt}{\int_0^\infty C(x=L,t)\,dt}. \quad (34)$$

In this study, the first three moments are calculated for the equilibrium dispersive and lumped kinetic models. The formulas for the finite moments μ_0, μ_1, μ_2', μ_3' corresponding to the EDM and LKM with both sets of boundary conditions are given in Table 1. Complete derivations of these moments for EDM and LKM are presented in Appendix A. It is well known that the first moment μ_1 corresponds to the retention time t_R. The value of the equilibrium constant a can be estimated from the slopes of a straight lines, $\mu_1 = t_R$ over $1/u$ for constant column length and porosity. It is shown (cf. Table 1) that effects of longitudinal diffusion are not significant with respect to retention time or first moment. The second central moment μ_2 or the variance of the elution breakthrough curves or peaks provides significant information related to mass transfer processes in the column. The quantitative value of μ_2 or variance indicates the band broadening or width of breakthrough curves or peaks and helps to calculate the HETP (height equivalent to theoretical plates). A zeroth value of third statistical moment μ_3' designates symmetric curves. Finally, the third central moment μ_3' was analyzed which evaluates front asymmetries. The second and the third central moments for the more general Danckwerts BCs reduce to the moments for the Dirichlet BCs in case D_{app} approaches to zero. A comparison of analytical moments and numerical moments obtained by the proposed numerical scheme is given in the next section.

5. Numerical scheme for solving LKM

In this section, the Runge Kutta discontinuous Galerkin method is applied to lumped kinetic model, e.g. Cockburn and Shu (1989, 2001). The scheme is second order accurate in the axial-coordinate. The resulting ODE-system is solved by using a third-order Runge–Kutta ODE-solver. For simplicity, a single

Table 1
Analytically determined moments for EDM and LKM for $x=1$ and $c_0=1$, $\mu_0=1$ and $\mu_1 = L/u(1+aF)$.

Models and BC's	μ_2'	μ_3'
EDM (Dirichlet)	$\frac{2LD_{app}(1+aF)^2}{u^3}$	$\frac{12LD_{app}^2}{u^5}(1+aF)^3$
EDM (Danckwerts)	$\frac{2LD_{app}}{u^3}(1+aF)^2\left[1+\frac{D_{app}}{Lu}(e^{-Lu/D_{app}}-1)\right]$	$\frac{12LD_{app}^2(1+aF)^3}{u^5}\left[\left(1+\frac{2D_{app}}{Lu}\right)e^{-Lu/D_{app}}+\left(1-\frac{2D_{app}}{Lu}\right)\right]$
LKM (Dirichlet)	$\frac{2LD(1+aF)^2}{u^3}+\frac{1}{k}\left(\frac{2LaF(1-\epsilon)}{u}\right)$	$\frac{12LD^2}{u^5}(1+aF)^3+\frac{1}{k}\left(\frac{12LD(1+aF)aF(1-\epsilon)}{u^3}\right)+\frac{1}{k^2}\left(\frac{6LaF(1-\epsilon)^2}{u}\right)$
LKM (Danckwerts)	$\frac{2LD}{u^3}(1+aF)^2\left[1+\frac{D}{Lu}(e^{-Lu/D}-1)\right]+\frac{1}{k}\left(\frac{2LaF\epsilon}{u}\right)$	$\frac{12LD^2(1+aF)^3}{u^5}\left[\left(1+\frac{2D}{Lu}\right)e^{-Lu/D}+\left(1-\frac{2D}{Lu}\right)\right]$ $+\frac{1}{k}\left[\frac{12LDaF\epsilon(1+aF)}{u^3}\left(\frac{D}{Lu}e^{-Lu/D}+F-\frac{D}{Lu}\right)\right]+\frac{1}{k^2}\left(\frac{6LaF^3\epsilon^2}{u}\right)$

component model is considered to derive the numerical scheme

$$\frac{\partial c}{\partial t}+\frac{\partial}{\partial z}\left(uc-D\frac{\partial c}{\partial z}\right)=-\frac{k}{\epsilon}(q^*-q), \tag{35}$$

$$\frac{\partial q}{\partial t}=\frac{k}{1-\epsilon}(q^*-q). \tag{36}$$

Let us define

$$g(c):=\sqrt{D}\frac{\partial c}{\partial z},\quad f(c,g):=uc-\sqrt{D}g(c). \tag{37}$$

Then, Eq. (35) changes to the following system of PDEs:

$$\frac{\partial c}{\partial t}=-\frac{\partial f}{\partial z}-\frac{k}{\epsilon}(q^*-q), \tag{38}$$

$$g=\sqrt{D}\frac{\partial c}{\partial z}, \tag{39}$$

$$\frac{\partial q}{\partial t}=\frac{k}{1-\epsilon}(q^*-q). \tag{40}$$

The axial-length variable z is discretized as follows. For $j=1,2,3,\ldots,N$, let $z_{j+\frac{1}{2}}$ be the cell partitions, $I_j=]z_{j-\frac{1}{2}},z_{j+\frac{1}{2}}[$ be the domain of cell j, $\Delta z_j=z_{j+\frac{1}{2}}-z_{j-\frac{1}{2}}$ be the width of cell j (cf. Fig. 1). Moreover, $I=UI_j$ be the partition of the whole domain. We seek an approximate solution $c_h(t,z)$ to $c(t,z)$ such that for each time $t\in[0,T]$, $c_h(t,z)$ belongs to the finite dimensional space

$$V_h=\{v\in L^1(I):v|_{I_j}\in P^m(I_j),\quad j=1,2,3,\ldots,N\}, \tag{41}$$

where $P^m(I_j)$ denotes the set of polynomials of degree up to m defined on the cell I_j. Note that in V_h, the functions are allowed to have jumps at the cell interface $z_{j+\frac{1}{2}}$. In order to determine the approximate solution $c_h(t,z)$, a weak formulation is needed. To obtain weak formulation, Eqs. (38)–(40) are multiplied by an arbitrary smooth function $v(z)$ followed by integration by parts over the interval I_j, we get

$$\int_{I_j}\frac{\partial c(t,z)}{\partial t}v(z)\,dz=-(f(c_{j+\frac{1}{2}},g_{j+\frac{1}{2}})v(z_{j+\frac{1}{2}})-f(c_{j-\frac{1}{2}},g_{j-\frac{1}{2}})v(z_{j-\frac{1}{2}}))+\int_{I_j}\left(f(c,g)\frac{\partial v(z)}{\partial z}\right)dz-\frac{k}{\epsilon}\int_{I_j}(q^*-q)v(z)\,dz, \tag{42}$$

$$\int_{I_j}g(c)v(z)\,dz=\sqrt{D}(c_{j+\frac{1}{2}}v(z_{j+\frac{1}{2}})-c_{j-\frac{1}{2}}v(z_{j-\frac{1}{2}}))-\sqrt{D}\int_{I_j}c(z)\frac{\partial v(z)}{\partial z}\,dz, \tag{43}$$

$$\int_{I_j}\frac{\partial q}{\partial t}v(z)\,dz=\frac{k}{1-\epsilon}\int_{I_j}(q^*-q)v(z)\,dz. \tag{44}$$

One way to implement Eq. (41) is to choose Legendre polynomials, $P_l(z)$, of order l as local basis functions. In this case, the L^2-orthogonality property of Legendre polynomials can be exploited, namely

$$\int_{-1}^{1}P_l(s)P_{l'}(s)=\left(\frac{2}{2l+1}\right)\delta_{ll'}. \tag{45}$$

For each $z\in I_j$, the solutions c_h and g_h can be expressed as

$$c_h(t,z)=\sum_{l=0}^{m}c_j^{(l)}\varphi_l(z),\quad g_h(c_h(t,z))=\sum_{l=0}^{m}g_j^{(l)}\varphi_l(z),$$

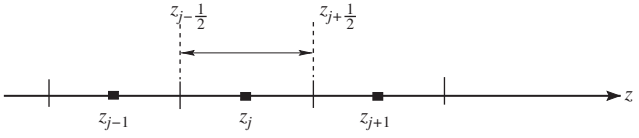

Fig. 1. Discretization of the computational domain.

$$q_h(t,z)=\sum_{l=0}^{m}q_j^{(l)}\varphi_l(z), \tag{46}$$

where

$$\varphi_l(z)=P_l(2(z-z_j)/\Delta z_j)),\quad l=0,1,\ldots,m. \tag{47}$$

If $m=0$ the approximate solution c_h uses the piecewise constant basis functions, if $m=1$ the linear basis functions are used, and so on. In this paper the linear basis functions are taken into account, therefore $l=0$, 1. By using Eqs. (45)–(47), it is easy to verify that

$$w_j^{(l)}(t)=\frac{2l+1}{\Delta z_j}\int_{I_j}w_h(t,z)\varphi_l(z)\,dz,\quad w\in\{c,g,q,q^*\}. \tag{48}$$

Then, the smooth function $v(z)$ can be replaced by the test function $\varphi_l\in V_h$ and the exact solutions c and g by the approximate solutions c_h and g_h. Moreover, the function $f(c_{j+\frac{1}{2}},g_{j+\frac{1}{2}})=f(c(t,z_{j+\frac{1}{2}}),g(c_{j+\frac{1}{2}}))$ is not defined at the cell interface $z_{j+\frac{1}{2}}$. Therefore, it has to be replaced by a numerical flux that depends on two values of $c_h(t,z)$ at the discontinuity, i.e.

$$f(c_{j+\frac{1}{2}},g_{j+\frac{1}{2}})\approx h_{j+\frac{1}{2}}=h(c_{j+\frac{1}{2}}^-,c_{j-\frac{1}{2}}^+). \tag{49}$$

As $g:=g(c)$, it can be dropped from the arguments of h for simplicity. Here

$$c_{j+\frac{1}{2}}^-:=c_h(t,z_{j+\frac{1}{2}}^-)=\sum_{l=0}^{m}c_j^{(l)}\varphi_l(z_{j+\frac{1}{2}}),$$
$$c_{j-\frac{1}{2}}^+:=c_h(t,z_{j-\frac{1}{2}}^+)=\sum_{l=0}^{m}c_j^{(l)}\varphi_l(z_{j-\frac{1}{2}}). \tag{50}$$

Using the above definitions, the weak formulations in Eqs. (42) and (43) simplify to

$$\frac{dc_j^{(l)}(t)}{dt}=-\frac{2l+1}{\Delta z_j}(h_{j+\frac{1}{2}}\varphi_l(z_{j+\frac{1}{2}})-h_{j-\frac{1}{2}}\varphi_l(z_{j-\frac{1}{2}}))+\frac{2l+1}{\Delta z_j}\int_{I_j}\left(f(c_h,g_h)\frac{d\varphi_l(z)}{dz}\right)-\frac{k}{\epsilon}(q_j^{*(l)}-q_j^{(l)}), \tag{51}$$

$$g_j^{(l)}(t)=\frac{2l+1}{\Delta z_j}\sqrt{D}\times\left(c_{j+\frac{1}{2}}\varphi_l(z_{j+\frac{1}{2}})-c_{j-\frac{1}{2}}\varphi_l(z_{j-\frac{1}{2}})-\int_{I_j}c_h(t,z)\frac{d\varphi_l(z)}{dz}\,dz\right), \tag{52}$$

$$\frac{dq_j^{(l)}(t)}{dt}=\frac{k}{1-\epsilon}(q_j^{*(l)}-q_j^{(l)}). \tag{53}$$

The initial data for the above system are given as, cf. Eq. (48),

$$c_j^{(l)}(0)=\frac{2l+1}{\Delta z_j}\int_{I_j}c(0,z)\varphi_l(z)\,dz,\quad g_j^{(l)}(0)=g(c_j^{(l)}(0)),$$
$$q_j^{(l)}(0)=q(c_j^{(l)}(0)). \tag{54}$$

It remains to choose the appropriate numerical flux function h. The above equation defines a monotone scheme if the numerical flux function $h(a,b)$ is consistent, $h(c,c)=f(c,g(c))$, and satisfies the Lipschitz continuity condition, i.e. $h(a,b)$ is a non-decreasing function of its first argument and non-increasing function of its second argument. In other words, a scheme is called monotone if it preserves the monotonicity of the numerical one-dimensional solution when passing from one time step to another. In this paper, the local Lax–Friedrichs flux was used which satisfies the above mentioned properties, see e.g. Kurganov and Tadmor (2000), LeVeque (2003), Zhang and Liu (2005)

$$h^{LLF}(a,b)=\frac{1}{2}[f(a,g(a))+f(b,g(b))-C(b-a)], \tag{55}$$

$$C=\max_{\min(a,b)\le s\le\max(a,b)}|f'(s,g(s))|. \tag{56}$$

The Gauss–Lobatto quadrature rule of order 10 was used to approximate the integral terms appearing on the right hand side of Eqs. (51) and (52).

In order to achieve the total variation stability, some limiting procedure has to be introduced. For that purpose, it is needed to modify $c^{\pm}_{j+\frac{1}{2}}$ in Eq. (49) by some local projection. For more details, see e.g. Cockburn and Shu (1989). To this end, we write (50) as

$$c^{-}_{j+\frac{1}{2}} = c^{(0)}_j + \tilde{c}_j, \quad c^{+}_{j-\frac{1}{2}} = c^{(0)}_j - \hat{c}_j, \tag{57}$$

where

$$\tilde{c}_j = \sum_{l=1}^{m} c^{(l)}_j \varphi_l(z_{j+\frac{1}{2}}), \quad \hat{c}_j = -\sum_{l=1}^{m} c^{(l)}_j \varphi_l(z_{j-\frac{1}{2}}). \tag{58}$$

In this study, we consider the linear basis functions, therefore $l=0, 1$. In above equation, when $m=0$, $\tilde{c}_j = \hat{c}_j = 0$ and when $m=1$, $\tilde{c}_j = \hat{c}_j = 6c^{(1)}_j$, etc. Next, $\tilde{c}_j$ and $\hat{c}_j$ can be modified as

$$\begin{aligned} \tilde{c}^{(\mathrm{mod})}_j &= \mathrm{mm}(\tilde{c}_j, \Delta_+ c^{(0)}_j, \Delta_- c^{(0)}_j), \\ \hat{c}^{(\mathrm{mod})}_j &= \mathrm{mm}(\hat{c}_j, \Delta_+ c^{(0)}_j, \Delta_- c^{(0)}_j), \end{aligned} \tag{59}$$

where $\Delta_{\pm} := \pm(c_{j\pm1} - c_j)$ and mm is the usual minmod function defined as

$$\mathrm{mm}(a_1,a_2,a_3) = \begin{cases} s \cdot \min\limits_{1\le i\le 3} |a_i| & \text{if } \mathrm{sign}(a_1) = \mathrm{sign}(a_2) = \mathrm{sign}(a_3) = s, \\ 0 & \text{otherwise.} \end{cases} \tag{60}$$

Then, Eq. (57) modifies to

$$c^{-(\mathrm{mod})}_{j+\frac{1}{2}} = c^{(0)}_j + \tilde{c}^{(\mathrm{mod})}_j, \quad c^{+(\mathrm{mod})}_{j-\frac{1}{2}} = c^{(0)}_j - \hat{c}^{(\mathrm{mod})}_j \tag{61}$$

and replaces (49) by

$$h_{j+\frac{1}{2}} = h(c^{-(\mathrm{mod})}_{j+\frac{1}{2}}, c^{+(\mathrm{mod})}_{j-\frac{1}{2}}). \tag{62}$$

This local projection limiter does not affect the accuracy in the smooth regions and convergence can be achieved without oscillations near shocks, e.g. Cockburn and Shu (1989). Finally, a Runge–Kutta method that maintains the TVB property of the scheme is needed to solve the resulting ODE-system. Let us rewrite Eqs. (51) and (53) in a concise form as

$$\frac{dc_h}{dt} = L_h(c_h, t). \tag{63}$$

Then, the m-order TVB Runge–Kutta method can be used to approximate Eq. (63)

$$\begin{aligned} (c_h)^m &= \sum_{l=0}^{m-1} [\alpha_{ml}(c_h)^{(l)} + \beta_{ml}\Delta t L_h((c_h)^{(l)}, t^s + d_l\Delta t)], \\ & m = 1,2,\ldots,r, \end{aligned} \tag{64}$$

where based on Eq. (54)

$$(c_h)^{(0)} = (c_h)^m, \quad (c_h)^{(r)} = (c_h)^{m+1}. \tag{65}$$

Here, s denotes the s-th time step. For second order TVB Runge–Kutta method the coefficients are given as

$$\begin{aligned} &\alpha_{10} = \beta_{10} = 1, \quad \alpha_{20} = \alpha_{21} = \beta_{21} = \tfrac{1}{2}, \\ &\beta_{20} = 0, \quad d_0 = 0, \quad d_1 = 1. \end{aligned} \tag{66}$$

While, for the third order TVB Runge–Kutta method the coefficients are given as

$$\begin{aligned} &\alpha_{10} = \beta_{10} = 1, \quad \alpha_{20} = \tfrac{3}{4}, \quad \beta_{20} = 0, \quad \alpha_{21} = \beta_{21} = \tfrac{1}{4}, \quad \alpha_{30} = \tfrac{1}{3}, \\ &\beta_{30} = \alpha_{31} = \beta_{31} = 0, \quad \alpha_{32} = \beta_{32} = \tfrac{2}{3}; \quad d_0 = 0, \quad d_1 = 1, \quad d_2 = \tfrac{1}{2}. \end{aligned} \tag{67}$$

The CFL condition is given as

$$\Delta t \le \left(\frac{1}{2m+1}\right)\frac{\Delta z_j}{|u|}, \tag{68}$$

where $m=1, 2$ for second- and third-order schemes, respectively.

Boundary conditions: Let us put the boundary at $z_{-\frac{1}{2}} = 0$. The left boundary condition given by Eqs. (10a) and (10b) can be implemented as

$$c^{-}_{-\frac{1}{2}}(t) = c^{(0)}_0 + \frac{D}{u}\frac{c^{(0)}_1 - c^{(0)}_0}{\Delta z}, \tag{69}$$

$$\begin{aligned} \tilde{c}^{(\mathrm{mod})}_0 &= \mathrm{mm}(\tilde{c}_0, \Delta_+ c^{(0)}_0, 2(c^{(0)}_0 - c^{inj})), \\ \hat{c}^{(\mathrm{mod})}_0 &= \mathrm{mm}(\hat{c}_0, \Delta_+ c^{(0)}_0). \end{aligned} \tag{70}$$

Outflow boundary condition is used on the right end of the column, $c^{(l)}_{N+1} = c^{(l)}_N$.

6. Numerical test problems

In order to validate the results, several numerical test problems are solved. Here, linear basis functions are considered in each cell, giving a second order accurate DG-scheme in axial-coordinate. The ODE-system is solved by a third-order Runge–Kutta method given in Eq. (66). The program is written in the C-language under a Linux operating system and was compiled on a computer with an Intel(R) Core 2 Duo processor of speed 2 GHz and memory (RAM) 3.83 GB.

6.1. Single component breakthrough curves for linear isotherms

6.1.1. Error analysis for LKM

Here, a comparison of different numerical schemes is presented for lumped kinetic model. The parameters of the problem are given in Table 2. The Koren (1993) scheme was already presented by Javeed et al. (2011) for the EDM and the remaining flux limiters are given in Table 3. The numerical results at the column outlet are shown in Fig. 2. In that figure, the concentration profiles generated by using different numerical schemes on 100 grid points are compared with the analytical solution obtained from the Laplace transformation. It can be observed that DG and Koren methods have better accuracy as compared to other flux limiting finite volume schemes. Further, the zoomed plot of Fig. 2 shows that the solution of DG-scheme is closest to the analytical solution. The L^1-error in time at the column outlet was calculated

Table 2
Parameters for Section 6.1 (linear isotherm).

Parameters	Values
Column length	$L = 1.0$ m
Porosity	$\epsilon = 0.4$
Interstitial velocity	$u = 0.1$ m/s
Characteristic time	$\tau_C = 10$ s
Dispersion coefficient for EDM	$D_{app} = 10^{-4}$ m^2/s
Peclet no for EDM	$\tilde{\tau_1} = Pe = 10^3$
Characteristic time for EDM	$\tau_D = 0.01$ s
Dispersion coefficient for LKM	$D = 10^{-5}$ m^2/s
Peclet no for LKM	$\tilde{\tau_1} = Pe = 10^4$
Characteristic time for LKM	$\tau_D = 0.001$ s
Mass transfer coefficient	$k = 100$ 1/s
Characteristic time	$\tau_{MT} = 0.01$ s
Dimensionless number	$\tilde{\tau_2} = 10^3$
Concentration at inlet	$c_{1,0} = 1.0$ g/l
Henry coefficient	$a = 0.85$

using the formula

$$L^1\text{-error} = \sum_{n=1}^{N_T} |c_R^n - c_N^n| \Delta t. \tag{71}$$

The relative error can be defined as

$$\text{relative error} = \frac{\sum_{n=1}^{N_T} |c_R^n - c_N^n|}{\sum_{n=1}^{N_T} |c_R^n|} \Delta t, \tag{72}$$

where c_R^n denotes the Laplace solution at the column outlet for time t_n and c_N^n represents the corresponding numerical solution. Moreover, N_T denotes the total number of time steps and Δt represents the time step size. Note that, numerical accuracy can be influenced by the choice of time step size Δt. Comparisons of L^1-errors, relative errors, and computational times of schemes are given in Tables 4 and 5 for 50 and 100 grid points, respectively. It can be observed that the DG-scheme produces small errors compared to the other schemes for both 50 and 100 grid cells, but efficiency (or CPU time) of the Koren scheme is better than the other schemes for both numbers of grid points. It can be noticed that relative errors of the DG and Koren schemes are very low for 100 grid points. For that reason, to achieve reliable results with better accuracy, 100 mesh points are chosen for further numerical simulations discussed in this section. On the basis of these results, one can clearly conclude that the DG method can be an optimal choice to approximate chromatographic models. Therefore, we are relying on the results of the DG scheme for the remaining problems of this paper.

6.1.2. Dispersion and mass transfer effects

In this next problem, both the single component EDM and LKM models are considered and compared. The parameters used to solve the model equations are taken from Lim and Jorgen (2009) and are given in Table 2. Fig. 3 (top: left) depicts the dispersion effects of EDM by considering different values of D_{app} or characteristic times τ_D. It demonstrates that smaller values of D_{app} produce steeper fronts. Fig. 3 (top: right) shows similar dispersion effects by varying D as described by the LKM keeping $\tau_C = 10$ s and $\tau_{MT} = 0.01$ s ($k = 100$ 1/s, $\tilde{\tau_2} = 10^3$) fixed. The similarity with the corresponding figure for the EDM is due to the relative large value for k. In Fig. 3 (bottom: left), different values of the mass transfer coefficients k for fixed $D = 10^{-5}$ m^2/s ($Pe = 10^4$) and $\tau_C = 10$ s are used for the LKM. This figure shows that increasing values of k has a similar effects as produced by decreasing D. In Fig. 3 (bottom: right), dispersion coefficient $D = 10^{-3}$ m^2/s ($Pe = 10^2$) is taken into consideration for different values of k. It is evident that even for a large magnitude of the mass transfer coefficient k, sharp fronts are not possible due to significant dispersion effects. All trends generated numerically are well-known and realistic for the adsorption community.

6.1.3. Comparison of analytical and numerical solutions

This part focuses on the comparison of analytical and numerical results from the EDM and the LKM for both Dirichlet and Danckwerts boundary conditions. In Fig. 4 (left), the exact solution obtained for the EDM with Dirichlet boundary conditions is compared with the numerical Laplace inversion and DG-scheme

Table 3
Different flux limiters.

Flux limiter	Formula
Van Leer (Leer, 1977)	$\varphi(r) = \frac{\lvert r\rvert + r}{1 + \lvert r\rvert}$
Superbee (Roe, 1986)	$\varphi(r) = \max(0, \min(2r, 1), \min(r, 2))$
Minmod (Roe, 1986)	$\varphi(r) = \max(0, \min(1, r))$
MC (Leer, 1977)	$\varphi(r) = \max(0, \min(2r, \frac{1}{2}(1+r), 2))$

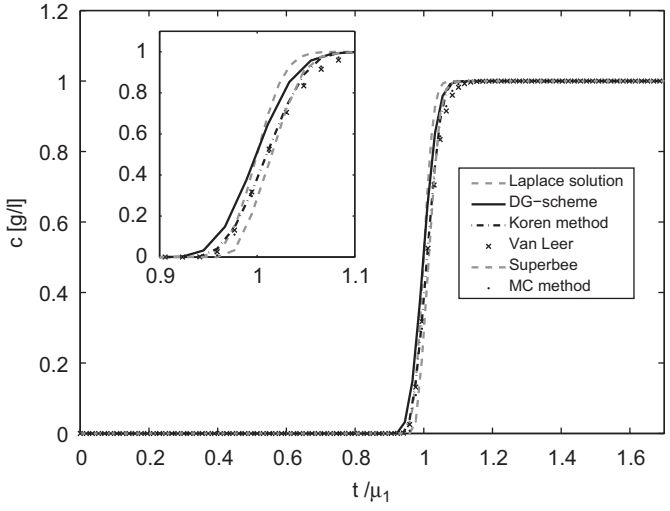

Fig. 2. Breakthrough curves (BTC) at $x = 1$. Comparison of different numerical schemes for LKM with $\tau_C = 10$ s, $\tau_D = 0.01$ s ($D = 10^{-5}$ m^2/s or $\tilde{\tau_1} = Pe = 1000$), and $\tau_{MT} = 0.01$ s ($k = 100$ 1/s or $\tilde{\tau_2} = 10^3$).

Table 4
Errors and CPU times at 50 grid points for linear isotherm.

Limiter	L^1-error	Relative error	CPU (s)
DG-scheme	0.4011	0.0100	5.86
Koren	0.5155	0.0137	4.90
Van Leer	0.9324	0.0248	8.26
Superbee	1.0732	0.0286	9.34
MC	0.9762	0.0260	8.82

Table 5
Errors and CPU times at 100 grid points for linear isotherm.

Limiter	L^1-error	Relative error	CPU (s)
DG-scheme	0.0139	3.71×10^{-4}	8.46
Koren	0.0153	4.08×10^{-4}	7.82
Van Leer	0.2255	0.0060	14.90
Superbee	0.2966	0.0079	17.73
MC	0.2477	0.0066	14.96

Table 6
Parameters for Section 6.2 (non-linear isotherm).

Parameters	Values
Column length	$L = 1.0$ m
Porosity	$\epsilon = 0.4$
Interstitial velocity	$u = 0.1$ m/s
Dispersion coefficient	$D = 10^{-4}$ m^2/s
Adsorption rate	$k = 10^3$ 1/s
Characteristic time	$\tau_C = 10$ s
Characteristic time	$\tau_D = 0.01$ s
Characteristic time	$\tau_{MT} = 0.001$ s
Peclet no	$\tilde{\tau_1} = Pe = 10^3$
Dimensionless number	$\tilde{\tau_2} = 10^4$
Concentrations	$c_{1,0} = c_{2,0} = 10$ mol/l
Henry coefficients	$a_1 = 0.5$, $a_2 = 1$
Constants used in Eq. (6)	$b_1 = 0.05$ l/mol, $b_2 = 0.1$ l/mol
Injection time	$t^{\text{in}} = 12$ s

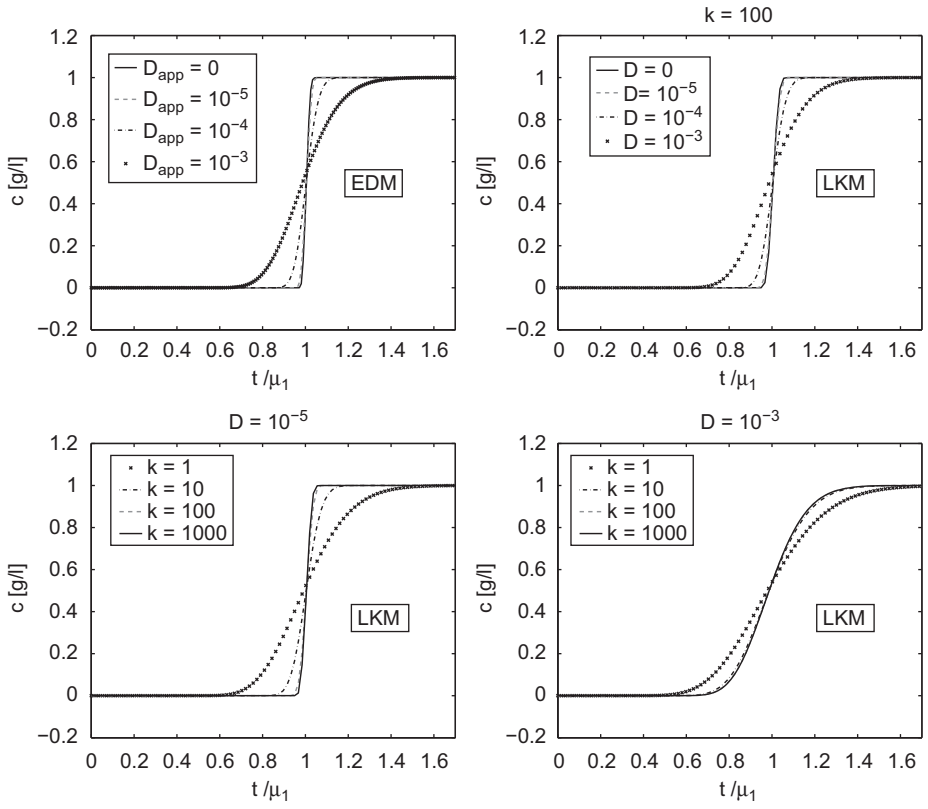

Fig. 3. BTC at $x=1$. Top (left): Dispersion effects as described by EDM keeping $\tau_C = 10$ s constant and varying τ_D (or D_{app}). Top (right): Dispersion effects for LKM keeping $\tau_C = 10$ s and $\tau_{MT} = 0.01$ s ($k = 100$ 1/s or $\tilde{\tau_2} = 10^3$) constant, and varying τ_D (or D). Bottom (left): Mass transfer effects for LKM taking $\tau_C = 10$ s, $\tau_D = 0.001$ s ($D = 10^{-5}$ m^2/s or $\tilde{\tau_1} = Pe = 10^4$), and varying τ_{MT} (or k). Bottom (right): Mass transfer effects taking $\tau_C = 10$ s, $\tau_D = 0.1$ s ($D = 10^{-3}$ m^2/s or $Pe = 10^2$), and varying τ_{MT} (or k).

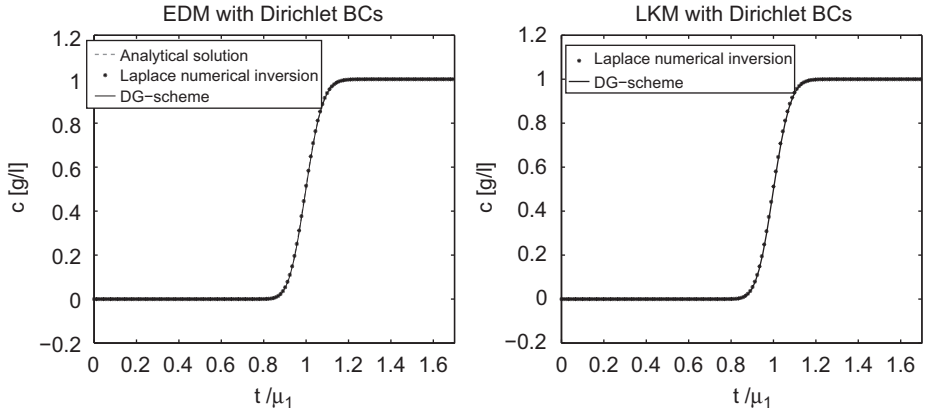

Fig. 4. BTC at $x=1$. EDM predictions using Dirichlet boundary conditions (9a), left: comparison of analytical solution (cf. Eq. (19)), Laplace numerical inversion and DG-method solutions with $\tau_C = 10$ s, $\tau_D = 0.02$ s ($D_{app} = 2 \times 10^{-4}$ m^2/s or $Pe = 500$). LKM predictions using Dirichlet boundary conditions (9a), right: comparison of Laplace numerical inversion and DG-scheme solutions with $\tau_C = 10$ s, $\tau_D = 0.01$ s ($D = 10^{-4}$ m^2/s or $Pe = 1000$), and $\tau_{MT} = 0.0667$ s ($k = 15$ 1/s or $\tilde{\tau_2} = 150$).

results. Good agreement of these profiles verifies the accuracy of numerical Laplace inversion and the proposed numerical scheme. Moreover, the numerical Laplace inversion technique is found to be a reliable method to solve such model problems and will be used below in the subsequent case studies. In Fig. 4 (right), the results of the DG method for the LKM and Dirichlet boundary conditions are compared with the numerical Laplace inversion solution. No analytical back transform solution was available for the LKM using Dirichlet boundary conditions. Fig. 5 (left) and (right) validates the results of numerical Laplace inversion and the DG-scheme for the EDM and LKM with Danckwerts boundary conditions, respectively. These profiles show the high precision of the numerical Laplace inversion technique and the suggested numerical scheme. Thus, it can also be concluded that the considered numerical Laplace inversion technique is an effective tool for solving these linear models.

6.1.4. *Effect of boundary conditions*

For the sake of generality, the Peclet number, cf. Eq. (13), is taken as parameter, while $\tilde{\tau_2} = 10^3$ ($\tau_{MT} = 0.01$ s) and $\tau_C = 10$ s are assumed to be constant for this problem. The results shown in

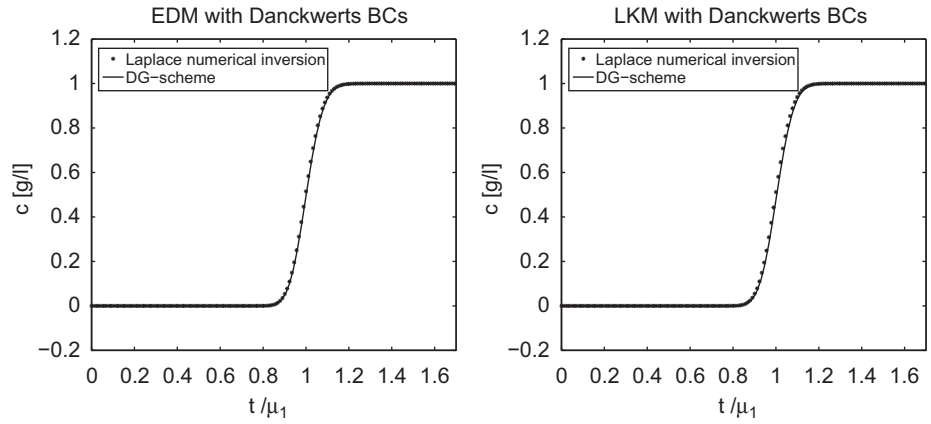

Fig. 5. BTC at $x=1$. EDM predictions using Danckwerts boundary conditions (10a), left: comparison of Laplace numerical inversion and DG-method solutions with $\tau_C = 10$ s, $\tau_D = 0.02$ s ($D_{app} = 2 \times 10^{-4}$ m^2/s or $Pe = 500$). LKM predictions using Danckwerts boundary conditions (10a), right: comparison of Laplace numerical inversion and DG-scheme solutions with $\tau_C = 10$ s, $\tau_D = 0.01$ s ($D = 10^{-4}$ m^2/s or $Pe = 1000$), and $\tau_{MT} = 0.0667$ s ($k = 15$ 1/s or $\tilde{\tau_2} = 150$).

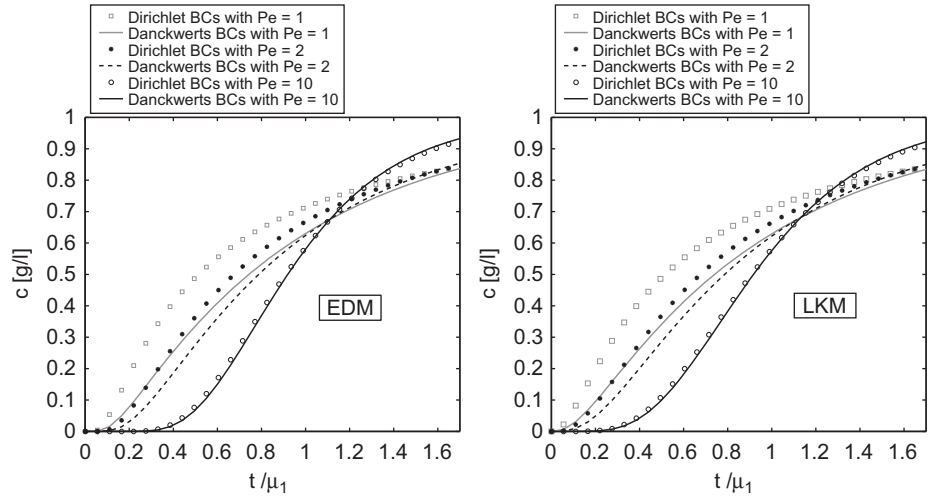

Fig. 6. BTC at $x=1$. Effect of boundary conditions for different values of Peclet number. Symbols are used for Dirichlet BCs (9a) and solid lines for Danckwerts BCs (10a), left: EDM with $\tau_C = 10$ s, and Pe or τ_D varies, right: LKM with $\tau_C = 10$ s, $\tau_{MT} = 0.01$ s ($k = 100$ 1/s or $\tilde{\tau_2} = 10^3$), and Pe or τ_D varies.

Fig. 6 illustrate the importance of using more accurate Danckwerts boundary conditions for chromatographic model equations, in the case of relatively small Peclet numbers, e.g. $Pe < 10$. For such values, there are visible differences between the results obtained by using Dirichlet and Danckwerts boundary conditions. On the basis of these results, one can conclude that the implementation of Dirichlet boundary conditions is not adequate for large dispersion coefficients. For large values of Peclet number ($Pe \gg 10$) or small axial dispersion coefficients as typically encountered in chromatographic columns well packed with small particles, there is no difference between Dirichlet and Danckwerts boundary conditions. The described behavior was observed in the solutions of both EDM and LKM.

6.1.5. Discussion on analytically and numerically determined moments

In this work, only step inputs are taken into account. The analytical moments are calculated by the formulas presented in Table 1 and in Appendix Appendix A. The formulas given below use derivatives to approximate the moments and transform the step response to a pulse response which is the requirement for finite results of numerical integration. The simulated moments are obtained from our proposed numerical methods by using the following formulas for the first normalized, second central and third central moments, respectively:

$$\mu_1 = \frac{\int_0^\infty \frac{dC(x=1,t)}{dt} t\, dt}{\int_0^\infty \frac{dC(x=1,t)}{dt}\, dt}, \quad \mu_2' = \frac{\int_0^\infty \frac{dC(x=1,t)}{dt} (t-\mu_1)^2\, dt}{\int_0^\infty \frac{dC(x=1,t)}{dt}\, dt},$$

$$\mu_3' = \frac{\int_0^\infty \frac{dC(x=1,t)}{dt} (t-\mu_1)^3\, dt}{\int_0^\infty \frac{dC(x=1,t)}{dt}\, dt}. \tag{73}$$

The trapezoidal rule is applied to approximate the integrals in Eq. (73). The quantitative comparison of first moment or (retention time) over the flow rate u for the EDM, LKM, and the analytical formula (cf. Table 1) can be seen in Fig. 7 (left). The results are in good agreement with each other, verify the high precision of our numerical results and reveal the expected linear trends.

For calculations of second moments μ_2' and third moments μ_3', the analytical formulas of Table 1 are used.

Matching μ'_{2EDM} and μ'_{2LKM} for the Dirichlet boundary conditions generates the following relationship between D_{app}, D and k:.

$$D_{app} = D + \frac{1}{k}\left(\frac{a(1-\epsilon)^2}{\epsilon\left(1+a\frac{(1-\epsilon)}{\epsilon}\right)^2}\right)u^2. \tag{74}$$

For given a, ϵ, and u, the above equation can be used to find possible connections between the kinetic parameters of two models which should provide very similar elution profiles. For given reference values of a and ϵ (cf. Table 2), for a velocity $u^* = 0.35$ m/s and a given $D_{app} = 10^{-4}$ m^2/s for EDM, there is an infinite number of combinations for k and D in the LKM. For example $D = 5 \times 10^{-5}$ m^2/s, we obtain $k = 362$ 1/s from the formula (74). The crossing point for the second moments of the two models marked in Fig. 8 (left) indicates that for this particular flow rate u^*, both models will produce almost the same concentration profiles, as verified in Fig. 8 (right). For other than this specific value of flow rate, keeping D_{app}, D, and k fixed, the results of equilibrium dispersive and lumped kinetic models should deviate from each other. This is clearly depicted in Fig. 8 (right) for $u = 0.1$ m/s.

To study the third moments in more detail, we varied u and increased the values of D_{app} and D by an order of magnitude, i.e. $D_{app} = 10^{-3}$ m^2/s and $D = 5 \times 10^{-4}$ m^2/s, and specified corresponding k values exploiting Eq. (74). Fig. 9 (left) shows the third moments μ'_3 for different flow rates and reveals the difference in the third moments for the perfect match of the second moments. A good agreement between analytical and numerical moments of our proposed numerical scheme guarantees the high precision of simulation results one more time. For velocity $u = 0.1$ m/s, where the large difference between two models is seen in Fig. 9 (left), time derivatives of two breakthrough curves for both models are plotted in Fig. 9 (right). It can be observed that EDM gives large values of μ'_3 as compared to LKM. Thus, EDM produces more asymmetry in the concentration profiles which is visible in Fig. 9 (right). The fronting edge is steeper and the tailing edge is more disperse for the EDM predictions as a clear indication of larger asymmetry compared to the LKM predictions (cf. Fig. 9 (right)). However, it is evident that the difference in the profiles of both models is still very small. This justifies the use of the simpler EDM for linear isotherm involving just one parameter D_{app} as compared to the more complicated LKM which involves two parameters D and k.

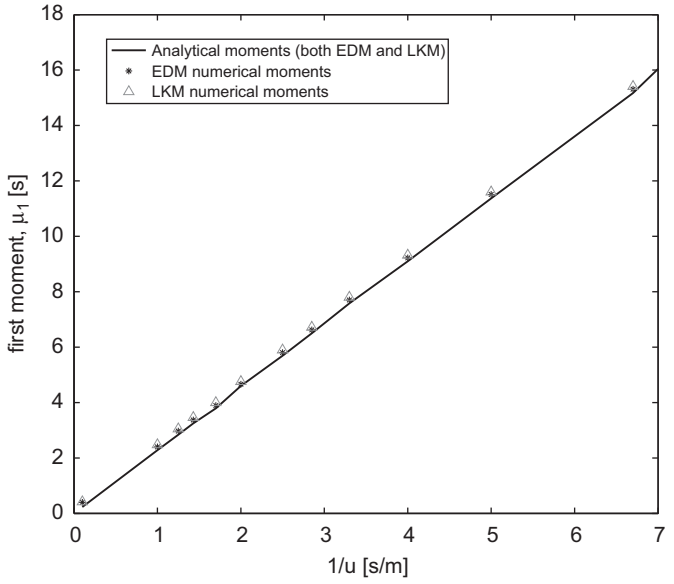

Fig. 7. First moments μ_1 of EDM and LKM versus different flow rates u. For EDM, Eq. (A.5) for analytical & Eq. (73) for numerical moments are used, considering $D_{app} = 10^{-4}$ m^2/s. For LKM, Eq. (A.25) for analytical & Eq. (73) for numerical moments are used, considering $D = 5 \times 10^{-5}$ m^2/s and $k = 30$ 1/s.

6.2. Two component elutions: extension to competitive non-linear adsorption isotherm and finite feed volumes (numerical simulations)

After validating the proposed numerical scheme for single component linear adsorption, this section is intended to extend our study to a non-linear problem. On the basis of accurate results for linear models, we concluded that the suggested numerical technique could produce reliable solutions for non-linear models as well. In this test problem, the two components lumped kinetic model along with a non-linear Langmuir isotherm (cf. Eq. (6)) is considered for finite feed volumes. A rectangular pulse of a liquid mixture of width $t^{in} \in [0,12]$ is injected to the column. The boundary conditions are given by Eqs. (10a) and (10b) for two components ($N_c = 2$). The parameters of this problem are taken from Shipilova et al. (2008) and are provided in Table 3. The numerical results are shown in Fig. 10 (left) by using 150 spatial grid points. The figure elucidates that the DG-scheme gives better resolution of the rectangular profiles as compared to the Koren scheme. These results also agree with those obtained by Shipilova et al. (2008), even for coarse mesh cells. The simulation results validate the importance of suggested method for approximating non-linear chromatographic models. Fig. 10 (right) describes non-equimolar injection concentrations with $c_{1,0} = 4$ mol/l and

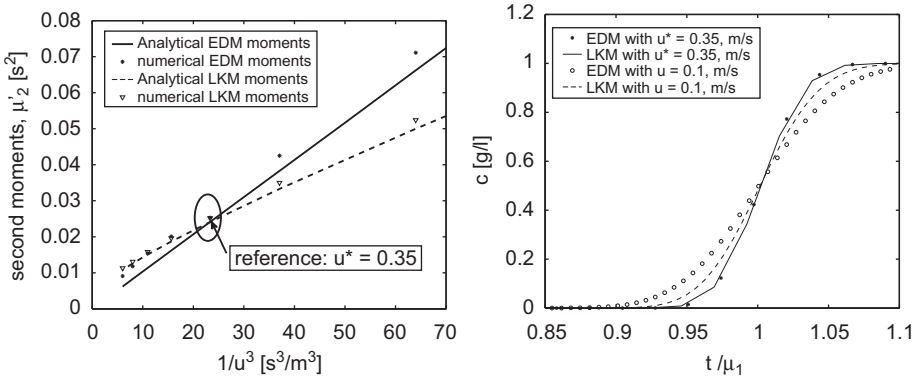

Fig. 8. Left: second moments μ'_2 for both models, analytical versus numerical with $D_{app} = 10^{-4}$ m^2/s for EDM, $D = 5 \times 10^{-5}$ m^2/s and $k = 362$ 1/s for LKM. Crossing at $u^* = 0.35$ m/s. Right: two predicted breakthrough curves for $u^* = 0.35$ m/s and $u = 0.1$ m/s, respectively.

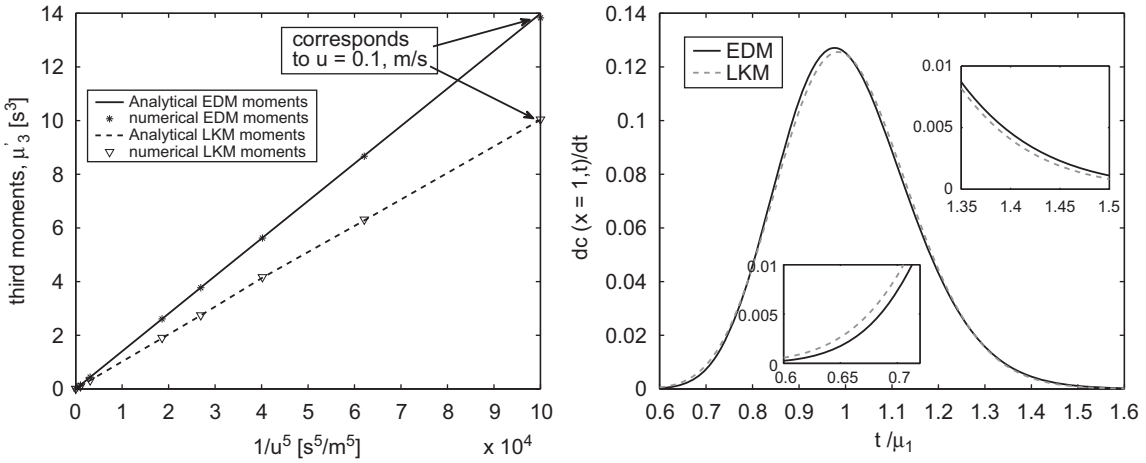

Fig. 9. Left: third moments μ_3' versus $1/u^5$. For EDM $D_{app}=10^{-3}$ m^2/s, and for LKM, $D=5\times10^{-4}$ m^2/s are used. Moreover, k is adjusted for each u via Eq. (74) to match μ_2'. Danckwerts BCs are taken into account. Right: Time derivatives of breakthrough curves. Illustration of effects of differences in third moments generated by EDM and LKM for $u=0.1$ m/s (corresponding to $1/u^5=10^5$).

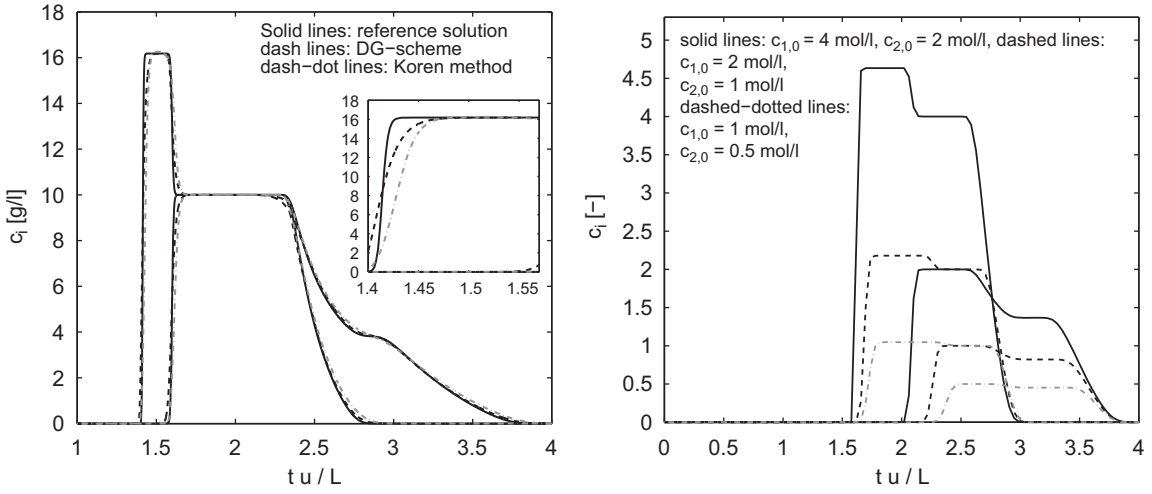

Fig. 10. Left: Two component non-linear elutions profile at the column outlet. Parameters are given in Table 6. Right: different injection volumes are used, first injection: $c_{1,0}=4$ mol/l and $c_{2,0}=2$ mol/l, second injection: $c_{1,0}=2$ mol/l and $c_{2,0}=1$ mol/l, third injection: $c_{1,0}=1$ mol/l, $c_{2,0}=0.5$ mol/l.

$c_{2,0}=2$ mol/l, $c_{1,0}=2$ mol/l and $c_{2,0}=1$ mol/l as well as $c_{1,0}=1$ mol/l and $c_{2,0}=0.5$ mol/l, respectively. The results in Fig. 10 (right) illustrate the well-known fact that strong non-linearities produce overshoots in the profiles. The efficiency and accuracy of the schemes can be graphically seen in Fig. 11. These plots highlight that errors of the DG-scheme are lower than the other schemes. It is probably worthwhile to conclude that an increase in the number of grid points produces smaller errors, but the computational time of the numerical schemes increases. The computational times of the DG and the Koren scheme are comparable, while the time taken by the other schemes is significantly higher. From the above observations, we conclude that the DG-scheme could be a better option for solving such models.

7. Conclusion

This paper described analytical and numerical investigations of equilibrium dispersive and lumped kinetic models by considering Dirichlet and Danckwerts boundary conditions. The Laplace transformation was used as a basic tool to transform the single-component linear sub model to a linear ordinary differential equation which is then solved analytically in the Laplace domain. The inverse numerical Laplace formula was employed to get back the time domain solution due to the unavailability of exact solution. A moments analysis of both models was carried out analytically and numerically for linear isotherms. Good agreement up to third moments assure the better accuracy of numerical solutions. The close connection between EDM and LKM was analyzed for linear isotherms, a concordance formula was derived and the strength of the simpler EDM was illustrated. For the numerical solution of considered models, the DG-scheme was applied. The presented scheme satisfies the TVB property and gives second-order accuracy. The method incorporates the ideas of numerical fluxes and slope limiters in a very natural way to capture the physically relevant discontinuities without producing spurious oscillations in their vicinity. The accuracy of proposed scheme was validated against flux-limiting finite volume schemes and analytical solutions for linear isotherms. The DG-scheme was found to be a suitable method for the simulation of linear and non-linear chromatographic processes in terms of accuracy and efficiency.

The present contribution was focused on the numerical approximation of chromatographic process in a single column.

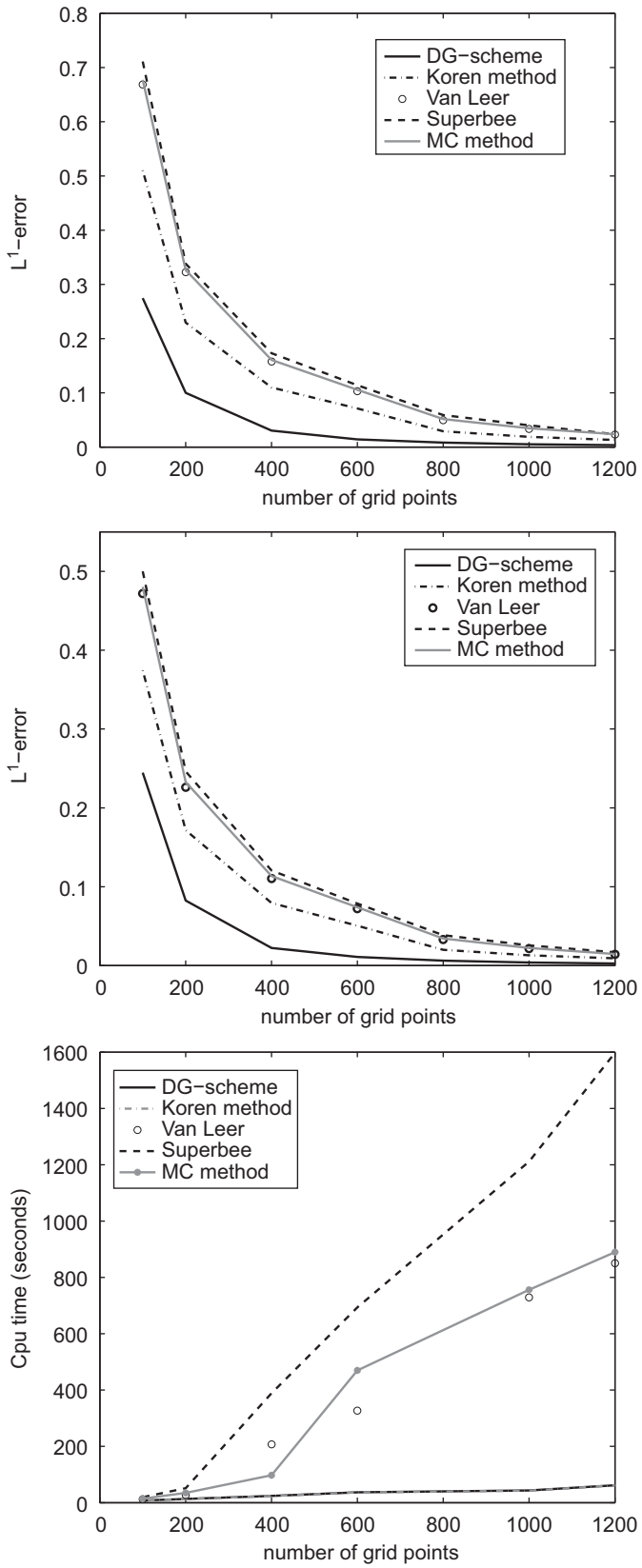

Fig. 11. Error analysis for two component non-linear elutions: top: L^1-Error for component 1, middle: L^1-Error for component 2, bottom: CPU time of different schemes. Parameters are given in Table 6.

However, the current scheme can also be used to deal with the non-linearity of more complicated processes, such as multi-column, moving-bed, and periodic operations. Especially, to develop an efficient and accurate numerical scheme for simulated moving bed will be the main focus of our future research work.

Nomenclature

a_n	Henry constants of component n, (–)
c_n	liquid phase concentration of component n, (mol/l)
d	column diameter, (m)
D_{app}	apparent dispersion coefficient in EDM, (m^2/s)
D	dispersion coefficient in LKM, (m^2/s)
h	numerical flux function
I_j	jth mesh interval, (–)
k	mass transfer coefficient, (1/s)
L	column length, (m)
mm	minmod limter function
N_c	number of components, (–)
N	number of grid cells, (–)
Pe	Peclet number, (–)
P_l	Legendre polynomial of order l (–)
q_n^*	solid phase concentration of component n, (mol/l)
t	time, (s)
u	interstitial velocity, (m/s)
x	dimensionless distance, $x = z/L$
z	spatial coordinate, (m)

Greek symbols

Δt	time step
Δx_j	width of mesh interval I_j
Δz_j	width of mesh interval I_j
ϵ	external porosity
τ_C	characteristic time (L/u), (1/s)
τ_D	characteristic time (D/u^2), (1/s)
τ_{MT}	characteristic time ($1/k$), (1/s)
ϕ_l	local basis function of order l
μ_n	n-th initial normalized moment
μ'_n	n-th central moment

Subscripts

in	injection
j	number of discretized cells
n	number of N_c components

Abbreviations

BCs	boundary conditions
DG	discontinuous Galerkin
EDM	equilibrium dispersive model
LKM	lumped kinetic model
ODEs	ordinary differential equations
PDEs	partial differential equations
RKDG	Runge–Kutta discontinuous Galerkin
TVB	total variation boundedness

Acknowledgment

The authors gratefully acknowledge the International Max Planck Research School Magdeburg and the Higher Education Commission (HEC) of Pakistan for financial support.

Appendix A

Here, the complete derivations of moments are presented for both equilibrium dispersive and lumped kinetic models with Dirichlet and Danckwerts boundary conditions.

A.1. Equilibrium dispersive model with Dirichlet boundary conditions

In this part, the moments of equilibrium dispersive model with Dirichlet boundary conditions are derived. By taking $x=1$ and $c_0=1$, the Eq. (18) can be written as

$$C(x=1,s)=\frac{1}{s}\exp\left(\frac{Pe}{2}-\frac{1}{2}\sqrt{Pe^2+4\,Pe\frac{L}{u}(1+aF)s}\right). \tag{A.1}$$

Let us define

$$Pe=\frac{Lu}{D_{app}},\quad b_1=Pe(1+aF)\frac{L}{u}. \tag{A.2}$$

The moment generating property of the Laplace transform is used exploiting (e.g. Van der Laan, 1958)

$$\mu_i=(-1)^i\lim_{s\to 0}\frac{d^i(sC)}{ds^i},\quad i=0,1,2,3,\ldots. \tag{A.3}$$

Thus, the zeroth moment is given as

$$\mu_0=\lim_{s\to 0}sC(x=1,s)=\lim_{s\to 0}\exp\left(\frac{Pe}{2}-\frac{1}{2}\sqrt{Pe^2+4b_1s}\right)=1. \tag{A.4}$$

The first initial moment can be obtained from Eq. (A.3) as

$$\mu_1=(-1)\lim_{s\to 0}\frac{d(sC)}{ds}=\lim_{s\to 0}\frac{\exp\left(\frac{Pe}{2}-\frac{1}{2}\sqrt{Pe^2+4b_1s}\right)b_1}{\sqrt{Pe^2+4b_1s}}, \tag{A.5}$$

Thus,

$$\mu_1=\frac{b_1}{Pe}=\frac{L}{u}(1+aF). \tag{A.6}$$

The second initial moment can be derived from the relation given in Eq. (A.3) as

$$\mu_2=(-1)^2\lim_{s\to 0}\frac{d^2(sC)}{ds^2}, \tag{A.7}$$

where

$$\frac{d^2(sC)}{ds^2}=\frac{2b_1^2\exp\left(\frac{Pe}{2}-\frac{1}{2}\sqrt{Pe^2+4b_1s}\right)}{(Pe^2+4a_1s)^{3/2}}+\frac{b_1^2\exp\left(\frac{Pe}{2}-\frac{1}{2}\sqrt{Pe^2+4b_1s}\right)}{Pe^2+4a_1s}. \tag{A.8}$$

Thus, the second initial moment is given as

$$\mu_2=\frac{b_1^2(2+Pe)}{Pe^3}=\frac{2L}{u^3}D_{app}(1+aF)^2+\frac{L^2}{u^2}(1+aF)^2. \tag{A.9}$$

The second central moment or the variance is given by the following expression:

$$\mu_2'=\mu_2-\mu_1^2=\frac{b_1^2}{Pe^3}=\frac{2L}{u^3}D_{app}(1+aF)^2. \tag{A.10}$$

Finally, the third initial moment is again obtained using Eq. (A.3)

$$\mu_3=(-1)^3\lim_{s\to 0}\frac{d^3(sC)}{ds^3}=\frac{b_1^3}{Pe^5}(6Pe+12+Pe^2) \tag{A.11}$$

or

$$\mu_3=\frac{L^3}{u^3}(1+aF)^3\left(\frac{6D_{app}}{Lu}+\frac{12D_{app}^2}{L^2u^2}+1\right). \tag{A.12}$$

The third central moment can be calculated from the moments given above using the subsequent formula

$$\mu_3'=\mu_3-3\mu_1\mu_2+2\mu_1^3. \tag{A.13}$$

Thus

$$\mu_3'=\frac{12LD_{app}^2}{u^5}(1+aF)^3. \tag{A.14}$$

A.2. Equilibrium dispersive model with Danckwerts boundary conditions

Here, the moments of the equilibrium dispersive model with Danckwerts boundary conditions are presented.

The zeroth moment is given as

$$\mu_0=\lim_{s\to 0}A\exp(\lambda_1x)+B\exp(\lambda_2x)=1. \tag{A.15}$$

The first initial moment is obtained as

$$\mu_1=\frac{b_1}{Pe}=\frac{L}{u}(1+aF). \tag{A.16}$$

The second initial moment is calculated as

$$\mu_2=\frac{2b_1^2}{Pe^4}\left(-1+Pe+\frac{Pe^2}{2}+e^{-Pe}\right) \tag{A.17}$$

or

$$\mu_2=\frac{2D_{app}^2(1+Fa)^2}{u^4}\left(-1+\frac{Lu}{D_{app}}+\frac{L^2u^2}{2D_{app}^2}+e^{-Lu/D_{app}}\right). \tag{A.18}$$

The second central moment is given as

$$\begin{aligned}\mu_2'&=\frac{2b_1^2e^{-Pe}}{Pe^4}(-e^{Pe}+e^{Pe}Pe+1)\\&=\frac{2L}{u^3}D_{app}(1+aF)^2\left(1+\frac{D_{app}}{Lu}(e^{-Lu/D_{app}}-1)\right).\end{aligned} \tag{A.19}$$

Lastly, the third initial moment is provided as

$$\mu_3=\frac{b_1^3}{Pe^6}(-24+6Pe+6Pe^2+Pe^3+24e^{-Pe}+18e^{-Pe}Pe). \tag{A.20}$$

The third central moment formula based on (A.13) is given below

$$\mu_3'=\frac{12LD_{app}^2(1+aF)^3}{u^5}\left[\left(1+\frac{2D_{app}}{Lu}\right)e^{-Lu/D_{app}}+\left(1-\frac{2D_{app}}{Lu}\right)\right]. \tag{A.21}$$

A.3. Lumped kinetic model with Dirichlet boundary conditions

This part presents the moments for the lumped kinetic model with Dirichlet boundary conditions. For $x=1$ and $c_0=1$, Eq. (30) can be rewritten as

$$C(x=1,s)=\frac{1}{s}\exp\left(\frac{b}{2}-\frac{1}{2}\sqrt{b^2+4a_1s-\frac{4a_2}{s+a3}+4a_4}\right). \tag{A.22}$$

With

$$\begin{aligned}&b=Pe=\frac{Lu}{D},\quad a_1=Pe\,\frac{L}{u},\quad a_2=\frac{L^2}{\epsilon D}\frac{k^2a}{(1-\epsilon)},\\&a_3=\frac{k}{(1-\epsilon)},\quad a_4=\frac{L^2ak}{\epsilon D}.\end{aligned} \tag{A.23}$$

The zeroth moment is given as

$$\mu_0=\lim_{s\to 0}\exp\left(\frac{b}{2}-\frac{1}{2}\sqrt{b^2+4a_1s-\frac{4a_2}{s+a3}+4a_4}\right)=1. \tag{A.24}$$

The first initial moment is calculated as

$$\mu_1 = \lim_{s\to 0} \frac{4\left(a_1+\frac{a_2}{(s+a_3)^2}\right)\exp\left(\frac{b}{2}-\frac{1}{2}\sqrt{b^2+4a_1 s-\frac{4a_2}{s+a_3}+4a_4}\right)}{4\sqrt{b^2+4a_1 s-\frac{4a_2}{s+a3}+4a_4}} \tag{A.25}$$

or

$$\mu_1 = \frac{a_1 a_3^2+a_2}{a_3^2 b} = \frac{L}{u}(1+aF). \tag{A.26}$$

The second initial moment is again derived using Eq. (A.7) with

$$\begin{aligned}\frac{d^2(sC)}{ds^2} = {} & \frac{4\left(a_1+\frac{a_2}{(s+a_3)^2}\right)\exp\left(\frac{b}{2}-\frac{1}{2}\sqrt{b^2+4a_1 s-\frac{4a_2}{s+a_3}+4a_4}\right)}{8\left(b^2+4a_1 s-\frac{4a_2}{s+a_3}+4a_4\right)^{3/2}} \\ & + \frac{2a_2\exp\left(\frac{b}{2}-\frac{1}{2}\sqrt{b^2+4a_1 s-4\frac{a_2}{s+a_3}+4a_4}\right)}{\left(b^2+4a_1 s-\frac{4a_2}{s+a_3}+4a_4\right)^{1/2}(s+a_3)^3} \\ & + \frac{4\left(a_1+\frac{a_2}{(s+a_3)^2}\right)\exp\left(\frac{b}{2}-\frac{1}{2}\sqrt{b^2+4a_1 s-\frac{4a_2}{s+a_3}+4a_4}\right)}{16\left(b^2+4a_1 s-\frac{4a_2}{s+a_3}+4a_4\right)}.\end{aligned} \tag{A.27}$$

Then

$$\mu_2 = \frac{1}{a_3^4 b^3}(2a_1^2 a_3^4+4a_1 a_3^2 a_2+2a_2^2+2a_2 a_3 b^2+b a_1^2 a_3^4+2b a_1 a_3^2 a_2+b a_2^2) \tag{A.28}$$

or

$$\begin{aligned}\mu_2 = {} & \frac{2LD(1+aF)^2}{u^3}+\frac{1}{k} \\ & \left(\frac{2LaF(1-\epsilon)}{u}+\frac{L^2}{u^2}(1+aF)^2\right).\end{aligned} \tag{A.29}$$

Exploiting Eq. (A.10), the second central moment is defined as

$$\begin{aligned}\mu_2' = {} & \frac{2}{a_3^4 b^3}(a_1^2 a_3^4+2a_1 a_3^2 a_2+a_2^2+a_2 a_3 b^2) \\ = {} & \frac{2LD\left(1+a\frac{1-\epsilon}{\epsilon}\right)^2}{u^3}+\frac{1}{k}\left(\frac{2La\frac{(1-\epsilon)^2}{\epsilon}}{u}\right)\end{aligned} \tag{A.30}$$

or

$$\mu_2' = \frac{2LD(1+aF)^2}{u^3}+\frac{1}{k}\left(\frac{2LaF(1-\epsilon)}{u}\right). \tag{A.31}$$

The third initial moment is obtained using again Eq. (A.11) with

$$\begin{aligned}-\frac{d^3(sC)}{ds^3} = {} & \frac{3\left(4a_1+\frac{4a_2}{(s+a_3)^2}\right)^3\exp\left(\frac{b}{2}-\frac{1}{2}\sqrt{b^2+4a_1 s-\frac{4a_2}{s+a_3}+4a_4}\right)}{16\left(b^2+4a_1 s-\frac{4a_2}{s+a_3}+4a_4\right)^{5/2}} \\ & + \frac{3a_2\left(4a_1+\frac{4a_2}{(s+a_3)^2}\right)\exp\left(\frac{b}{2}-\frac{1}{2}\sqrt{b^2+4a_1 s-\frac{4a_2}{s+a_3}+4a_4}\right)}{\left(b^2+4a_1 s-\frac{4a_2}{s+a_3}+4a_4\right)^{3/2}(s+a_3)^3} \\ & + \frac{3\left(4a_1+\frac{4a_2}{(s+a_3)^2}\right)^3\exp\left(\frac{b}{2}-\frac{1}{2}\sqrt{b^2+4a_1 s-\frac{4a_2}{s+a_3}+4a_4}\right)}{32\left(b^2+4a_1 s-\frac{4a_2}{s+a_3}+4a_4\right)^2} \\ & + \frac{6a_2\exp\left(\frac{b}{2}-\frac{1}{2}\sqrt{b^2+4a_1 s-\frac{4a_2}{s+a_3}+4a_4}\right)}{\left(b^2+4a_1 s-\frac{4a_2}{s+a_3}+4a_4\right)^{1/2}(s+a_3)^4} \\ & + \frac{3a_2\left(4a_1+\frac{4a_2}{(s+a_3)^2}\right)\exp\left(\frac{b}{2}-\frac{1}{2}\sqrt{b^2+4a_1 s-\frac{4a_2}{s+a_3}+4a_4}\right)}{2\left(b^2+4a_1 s-\frac{4a_2}{s+a_3}+4a_4\right)^{3/2}(s+a_3)^3} \\ & + \frac{\left(4a_1+\frac{4a_2}{(s+a_3)^2}\right)^3\exp\left(\frac{b}{2}-\frac{1}{2}\sqrt{b^2+4a_1 s-\frac{4a_2}{s+a_3}+4a_4}\right)}{64\left(b^2+4a_1 s-\frac{4a_2}{s+a_3}+4a_4\right)^{3/2}}.\end{aligned} \tag{A.32}$$

Then

$$\begin{aligned}\mu_3 = {} & \frac{1}{a_3^6 b^5}(12a_1^3 a_3^6+36a_1^2 a_3^4 a_2+36a_1 a_3^2 a_2^2+12a_2^3+12a_2 a_3^3 b^2 a_1 \\ & +12a_2^2 a_3 b^2+6b a_1^3 a_3^6+18b a_1^2 a_3^4 a_2+18b a_1 a_3^2 a_2^2+6b a_2^3+6a_2 a_3^2 b^4 \\ & +6a_2 a_3^3 b^3 a_1+6a_2^2 a_3 b^3+b^2 a_1^3 a_3^6+3b^2 a_1^2 a_3^4 a_2+3b^2 a_1 a_3^2 a_2^2+b^2 a_2^3)\end{aligned} \tag{A.33}$$

or

$$\begin{aligned}\mu_3 = {} & \frac{L^3}{u^3}(1+aF)^3\left(\frac{6D}{Lu}+\frac{12D^2}{L^2u^2}+1\right) \\ & +\frac{6L^2(1+aF)a(1-\epsilon)}{u^3 k}\left(\frac{2D}{L}+\frac{(1-\epsilon)u^2}{Lk(1+aF)}+u\right).\end{aligned} \tag{A.34}$$

Using (A.13), the third central moment is given as

$$\mu_3' = \frac{12LD^2}{u^5}(1+aF)^3+\frac{6L^2(1+aF)aF(1-\epsilon)}{ku^3}\left(\frac{2D}{L}+\frac{(1-\epsilon)u^2}{Lk(1+aF)}\right) \tag{A.35}$$

or

$$\mu_3' = \frac{12LD^2}{u^5}(1+aF)^3+\frac{1}{k}\left(\frac{12LD(1+aF)aF(1-\epsilon)}{u^3}\right)+\frac{1}{k^2}\left(\frac{6LaF(1-\epsilon)^2}{u}\right). \tag{A.36}$$

A.4. Lumped kinetic model with Danckwerts boundary conditions

This part discusses the derivation of moments for lumped kinetic model with Danckwerts boundary conditions.

The zeroth moment is again given as

$$\mu_0 = 1. \tag{A.37}$$

The first initial moment corresponding again to Eq. (A.6)

$$\mu_1 = \frac{a_1 a_3^2+a_2}{a_3^2 b} = \frac{L}{u}(1+aF). \tag{A.38}$$

The second initial moment is given as

$$\begin{aligned}\mu_2 = {} & \frac{e^{-b}}{a_3^4 b^4}(4a_1 a_3^2 a_2-2e^b a_1^2 a_3^4+2e^b b a_2^2+e^b b^2 a_2^2-4e^b a_1 a_3^2 a_2 \\ & +2e^b b a_1^2 a_3^4+e^b b^2 a_1^2 a_3^4+2a_2 e^b a_3 b^3+4e^b b a_1 a_3^2 a_2 \\ & +2e^b b^2 a_1^2 a_3^2 a_2+2a_1^2 a_3^4+2a_2^2-2be^b a_2^2).\end{aligned} \tag{A.39}$$

The second central moment is defined as, cf. (A.10)

$$\mu_2' = \frac{2L}{u^3}D(1+aF)^2\left(1+\frac{D}{Lu(e^{-Lu/D}-1)}\right) + \frac{1}{k}\left(\frac{2LaF\epsilon}{u}\right). \quad (A.40)$$

The third initial moment is given as

$$\begin{aligned}\mu_3 = \frac{e^{-b}}{a_3^6 b^6}(&24a_1^3a_3^6+24a_2^3+72a_1^2a_3^4a_2+72a_1a_3^2a_2^2\\ &+12a_2^2a_3b^2+18ba_1^3a_3^6\\ &+54ba_1^2a_3^4a_2+54ba_1^2a_3^2a_2^2+6a_2e^ba_3^2b^5+6a_1^3a_3^6e^bb^2\\ &-12a_2^2e^ba_3b^2+12a_2^2e^ba_3b^3\\ &+6e^bba_1^3a_3^6+6a_2^2a_3b^4+e^bb^3a_1^3a_3^6+18ba_2^3+6e^bba_2^3\\ &+e^bb^3a_2^3-24e^ba_1^3a_3^6\\ &+6e^bb^2a_2^3-24e^ba_2^3+18e^bba_1^2a_3^4a_2-12a_2e^ba_3^3b^2a_1\\ &+12a_2e^ba_3^3b^3a_1+18e^bba_1a_3^2a_2^2\\ &+6e^ba_2a_3^3b^4a_1+3e^bb^3a_1^2a_3^4a_2+3e^bb^3a_1a_3^2a_2^2+18a_1^2a_3^4e^bb^2a_2\\ &+18a_1a_3^2e^bb^2a_2^2\\ &-72e^ba_1^2a_3^4a_2-72e^ba_1a_3^2a_2^2+12a_2a_3^3b^2a_1).\end{aligned} \quad (A.41)$$

The third central moment is using again (A.13) as

$$\mu_3' = \frac{12LD^2(1+aF)^3}{u^5}\left[\left(1+\frac{2D}{Lu}\right)e^{-Lu/D}+\left(1-\frac{2D}{Lu}\right)\right] + \frac{1}{k}\left[\frac{12DLaF\epsilon(1+aF)}{u^3}\left(\frac{D}{Lu}e^{-Lu/D}+F-\frac{D}{Lu}\right)\right]+\frac{1}{k^2}\left(\frac{6LaF^3\epsilon^2}{u}\right). \quad (A.42)$$

References

Aizinger, V., Dawson, C., Cockburn, B., Castillo, P., 2000. Local discontinuous Galerkin method for contaminant transport. Adv. Water Res. 24, 73–87.

Bahhar, A., Baranger, J., Sandri, D., 1998. Galerkin discontinuous approximation of the transport equation and viscoelastic fluid flow on quadrilaterals. Numer. Meth. Partial Diff. Equations 14, 97–114.

Bassi, F., Rebay, S., 1997. A high-order accurate discontinuous finite element method for the numerical solution of the compressible Navier-Stokes equations. J. Comput. Phys. 131, 267–279.

Cockburn, B., Shu, C.-W., 1989. TVB Runge–Kutta local projection discontinuous Galerkin finite element method for conservation laws II. General framework. Math. Comput. 52, 411–435.

Cockburn, B., Hou, S., Shu, C.-W., 1990. TVB Runge–Kutta local projection discontinuous Galerkin finite element method for conservation laws IV: the multidimensional case. Math. Comput. 54, 545–581.

Cockburn, B., Cockburn, C.-W., 1998. The Runge–Kutta discontinuous Galerkin finite element method for conservation laws V: multidimensional systems. J. Comput. Phys. 141, 199–224.

Cockburn, B., Shu, C.-W., 2001. Runge–Kutta discontinuous Galerkin methods for convection-dominated problems. J. Sci. Comput. 16, 173–261.

Danckwerts, P.V., 1953. Continuous flow systems. Chem. Eng. Sci. 2, 1–9.

Felinger, A., Cavazzini, A., Dondi, F., 2004. Equivalence of the microscopic and macroscopic models of chromatography: stochastic-dispersive versus lumped kinetic model. J. Chromatogr. A 1043, 149–157.

Guiochon, G., Lin, B., 2003. Modeling for Preparative Chromatography. Academic Press.

Guiochon, G., Felinger, A., Shirazi, D.G., Katti, A.M., 2006. Fundamentals of Preparative and Nonlinear Chromatography, 2nd ed. ELsevier Academic Press, New York.

Holik, M., 2009. Application of discontinuous Galerkin method for the simulation of 3D inviscid compressible flows. In: Proceedings of the ALGORITMY, pp. 304–312.

Javeed, S., Qamar, S., Seidel-Morgenstern, A., Warnecke, G., 2011. Efficient and accurate numerical simulation of nonlinear chromatographic processes. Comput. Chem. Eng. 35, 2294–2305.

Koren, B., 1993. A robust upwind discretization method for advection, diffusion and source terms. In: Vreugdenhil, C.B., Koren, B. (Eds.), Numerical Methods for Advection–Diffusion Problems, Notes on Numerical Fluid Mechanics, vol. 45. Vieweg Verlag, Braunschweig, pp. 117–138. (Chapter 5).

Kurganov, A., Tadmor, E., 2000. New high-resolution central schemes for nonlinear conservation laws and convection–diffusion equations. J. Comput. Phys. 160, 241–282.

Kubin, M., 1965a. Beitrag zur Theorie der Chromatographie. Collect. Czech. Chem. Commun. 30, 1104–1118.

Kubin, M., 1965b. Beitrag zur Theorie der Chromatographie. 11. Einfluss der Diffusion Ausserhalb und der Adsorption Innerhalb des Sorbens- Korns. Collect. Czech. Chem. Commun. 30, 2900–2907.

Kucera, E., 1965. Contribution to the theory of chromatography: linear non-equilibrium elution chromatography. J. Chromatogr. A 19, 237–248.

Lapidus, L., Amundson, N.R., 1952. Mathematics of adsorption in beds, VI. The effect of longitudinal diffision in ion exchange and chromatographic columns. J. Phys. Chem. 56, 984–988.

Leer, B.V., 1977. Towards ultimate conservative finite difference scheme 4. A new approach to numerical convection scheme. J. Comput. Phys. 12, 276–299.

LeVeque, R.J., 2003. Finite Volume Methods for Hyperbolic Systems. Cambridge University Press, Cambridge.

Lim, Y.I., Jorgen, S.B., 2009. Performance evaluation of the conservation element and solution element method in the SMB process simulation. Chem. Eng. Process.: Process Intensification 59, 1931–1947.

Miyabe, K., Guiochon, G., 2000. Influence of the modification conditions of alkyl bonded ligands on the characteristics of reversed-phase liquid chromatography. J. Chromatogr. A 903, 1–12.

Miyabe, K., Guiochon, G., 2003. Measurement of the parameters of the mass transfer kinetics in high performance liquid chromatography. J. Sep. Sci. 26, 155–173.

Miyabe, K., 2007. Surface diffusion in reversed-phase liquid chromatography using silica gel stationary phases of different C1 and C18 ligand densities. J. Chromatogr. A 1167, 161–170.

Miyabe, K., 2009. Moment analysis of chromatographic behavior in reversed-phase liquid chromatography. J. Sep. Sci. 32, 757–770.

Rice, R.G., Do, D.D., 1995. Applied Mathematics and Modeling for Chemical Engineers. Wiley-Interscience, New York.

Roe, P.L., 1986. Characteristic-based schemes for the Euler equations. Ann. Rev. Fluid Mech. 18, 337–365.

Ruthven, D.M., 1984. Principles of Adsorption and Adsorption Processes. Wiley-Interscience, New York.

Reed, W.H., Hill, T.R., 1973. Triangular mesh methods for the neutron transport equation. Los Alamos Scientific Laboratory Report LA-UR, pp. 73–79.

Schneider, P., Smith, J.M., 1968. Adsorption rate constants from chromatography. A.I.Ch.E. J. 14, 762–771.

Seidel-Morgenstern, A., 1991. Analysis of boundary conditions in the axial dispersion model by application of numerical Laplace inversion. Chem. Eng. Sci. 46, 2567–2571.

Shipilova, O., Sainio, T., Haario, H., 2008. Particle transport method for simulation of multicomponent chromatography problems. J. Chromatogr. A 1204, 62–71.

Suzuki, M., Smith, J.M., 1971. Kinetic Studies by Chromatography. Chem. Eng. Sci. 26, 221–235.

Suzuki, M., 1973. Notes on determining the moments of the impulse response of the basic transformed equations. J. Chem. Eng. Jpn. 6, 540–543.

Van der Laan, Th., 1958. Letter to the editors on notes on the diffusion type model for the longitudinal mixing in flow. Chem. Eng. Sc. 7, 187–191.

Zhang, P., Liu, R.-X., 2005. Hyperbolic conservation laws with space-dependent fluxes: II. General study of numerical fluxes. J. Comput. Appl. Math. 176, 105–129.